Article

Selective Catalytic Reduction Catalyst Modeling for Control Purposes

Olov Holmer [ID] and Lars Eriksson *

Division of Vehicular Systems, Department of Electrical Engineering, Linköping University,
581 83 Linköping, Sweden
* Correspondence: lars.eriksson@liu.se

Abstract: In markets with strict emission legislations Selective Catalytic Reduction (SCR) has become the industry standard for NO_x abatement in heavy-duty vehicles, and therefore modeling and control of these systems are vital. Many SCR catalyst models are available in the literature and in this paper different models are discussed and classified into groups. Two models, based on the two most popular classes for control-oriented models, are implemented and compared with each other, one based on the continuously stirred-tank reactor approximation, and the other on a quasi-static behavior of the gas phase. The results show that assuming a quasi-static behavior of the gas phase in the catalyst gives better results in terms of accuracy and simulation time, especially when it comes to predictions of ammonia slip.

1. Introduction

Low fuel consumption is one of the most important factors to consider when developing a heavy-duty vehicle. However, the legislated requirements on emissions must also be met. The main objective is therefore to develop a powertrain with as low fuel consumption as possible, while still fulfilling the stringent emission legislations. This is achieved by both designing the hardware and developing control systems that optimally utilize this hardware. Currently, the trend in hardware is a fuel-efficient engine followed by an aftertreatment system that manages the emissions, and for NO_x reduction, Selective Catalytic Reduction (SCR) is the dominating technology for heavy-duty vehicles [1]. A major trend in control system development is model-based control, that is, a control system where a model is used within the control system or during its development. The thermal state of the SCR catalyst interacts with the dosing of urea and it is therefore important to model the energy flows and balances in the catalyst system. This highlights the importance of control-oriented SCR catalyst models.

1.1. SCR Catalyst Modeling

Most SCR catalyst models are based on the Eley–Rideal mechanism with reaction rates modeled using Arrhenius style equations. These models mainly differ in the way they handle the distribution of concentrations within the catalyst. This gives rise to a number of different classes of models and here the most commonly used for control purposes are treated.

1.1.1. One-Dimensional Models

As with most modeling, the modeling of an SCR catalyst starts with a number of assumptions. Common assumptions, that are used in most control-oriented models, are

- Incompressible flow of ideal gas

- Washcoat diffusion is assumed negligible/lumped into reaction rates
- A single channel represents the whole catalyst (homogeneous distribution and mix of the entering mass flow, no radial temperature gradient)

Using these assumptions, the SCR catalyst can be described using the one-dimensional partial differential equations in Section 2. Methods and software that solve these equations are available and this comprises the first class of models, herein called one-dimensional models. The high detail level of these models makes them slow to simulate, and therefore, they are most often used for fundamental studies of SCR catalysts. Like in [2] where a parameter study of how the geometry of the catalyst affects its efficiency is presented, or [3] where the effect of different inlet conditions on catalyst efficiency is investigated. Another example is [4] where the procedure of calibrating the model parameters is investigated.

More detailed models also exist, such as [5] where washcoat diffusion is considered. With the introduction of stricter emission legislations, the usage of these types of models can be assumed to increase [6,7]. However, since one-dimensional models are already too complex for control purposes, more detailed models are out of the scope here.

1.1.2. Continuously Stirred-Tank Reactor

By also assuming a homogeneous, continuously stirred, mix of gasses inside the catalyst the continuously stirred-tank reactor model is derived, see Section 3.2 for details. This model is used extensively for control-oriented purposes, such as state estimation [8] and predictive control [9–12].

By using multiple CSTR models in series, a more detailed model is achieved. Specifically, increasing from one to two segments gives large improvements [13].

1.1.3. Quasi-Static Models

The dynamics related to gas transport inside the catalyst are much quicker compared to other dynamics in the system. This results in a stiff problem, and it is therefore often assumed that the process exhibits a quasi-static behavior [14].

For the one-dimensional models this means that the PDEs related to the gas phase are transformed into ODEs, as described in Section 3.3. These models are reported to predict the behavior of the system very well [15] and are also capable of real-time implementation, with on-line state estimation as an example [16].

For CSTR models, the dynamic equations describing the gas conditions are transformed to algebraic equations. If only the standard SCR reaction is considered, a closed-form solution to the algebraic equations exist making an efficient implementation of the model possible, as observed in [17]. This model is used many different applications, for example: observer-based state-feedback [14], feed-forward and estimation [18], and predictive control [19]. In [20], a controller based on optimization is developed using a model where the NO_x conversion efficiency is modeled using a map.

1.1.4. Data-Driven Modeling

For most applications, data-driven models of SCR catalysts are available and used. The most common are maps, which can be used within the control system to determine the maximal amount of urea that can be allowed or to estimate the efficiency of the catalyst [21,22], or to describe specific parts of the model such as the NH_3 adsorption mechanism [23]. Another example is [24] where a neural network is trained to be used within an optimization scheme where the optimum amount of urea dosing is determined for different operating conditions. However, these models are usually tailored for specific applications and when it comes to more general purposes such as simulation of drive cycles, they are in general not applicable or inferior to physical-based models.

1.2. Problem Formulation

Numerous SCR catalyst models are available in the literature, as can be seen in Section 1.1. The focus in this paper is therefore on choosing a suitable model structure,

which is achieved by organizing the available models based on their structure and identifying the trends. The aim is to find, and implement, the most suitable model in terms of accuracy and simulation time for control purposes.

1.3. Contributions

The main contribution of this work is the detailed description and comparison between two common model classes for control-oriented SCR catalyst models. The work also contains the following major contributions:

1. A survey and classification of available models and the relationships between them,
2. a new way to include transport delay in one of the classes,
3. a tool generating implementations of the two model classes,
4. an investigation on how the discretization affects the model performance.

1.4. Outline

The remainder of this paper is organized as follows: In Section 1, the physical description of an SCR catalyst is presented, in Section 2 the spatial discretization of the catalyst is presented, in Section 3 an analysis of the steady-state solutions is presented, in Section 4 the temporal discretization is presented, in Section 5 the model generation tool is presented, in Section 6 the model generation tool is presented, in Section 7 the parameterization and validation of the models is discussed, in Section 8 the results are discussed, and in Section 9 conclusions are drawn.

2. Foundation from Physics

In this section, the one-dimensional partial differential equations that describe catalysts, and serve as a foundation for the models, are presented. The equations presented herein are a compilation based on a number of publications [2,16,25–28], and the reader is referred to these for more detailed information about the equations.
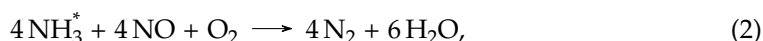
2.1. Working Principle of SCR

The basic principle behind an SCR is to reduce the amount of NO_x in the exhaust through reaction with a reducing agent, in this case ammonia, producing nitrogen gas and water.

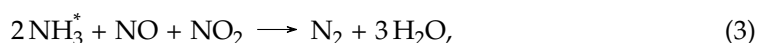2.1.1. Reactions in the SCR Catalyst

The reactions are usually described through the Eley–Rideal mechanism, with adsorption and desorption of NH_3 onto the catalyst surface

$$NH_3 \rightleftharpoons NH_3^*. \tag{1}$$

where $*$ denotes an adsorbed species. The adsorbed NH_3 reacts with the NO_x through one of the following NO_x reducing reactions: standard SCR

$$4\,NH_3^* + 4\,NO + O_2 \longrightarrow 4\,N_2 + 6\,H_2O, \tag{2}$$

fast SCR

$$2\,NH_3^* + NO + NO_2 \longrightarrow N_2 + 3\,H_2O, \tag{3}$$

and slow SCR

$$8\,NH_3^* + 6\,NO_2 \longrightarrow 7\,N_2 + 12\,H_2O. \tag{4}$$
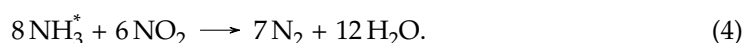
There are other, less essential reactions taking place in the catalyst, see [2,16,25–28] for a more complete list.

2.1.2. Reducing Agent

Urea-based SCR systems are the most common ones. In these systems, the NH_3 is derived from an aqueous urea solution of urea and water that is injected before the catalyst.

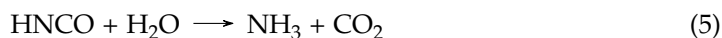The solution first evaporates after which the urea is decomposed to HNCO and NH_3. The HNCO is eventually also converted to NH_3 through hydrolysis

$$HNCO + H_2O \longrightarrow NH_3 + CO_2 \tag{5}$$

before and within the catalyst.

2.1.3. Dosing Control and Ammonia Slip

The amount of stored NH_3 in the catalyst affects its performance in that higher levels lead to higher conversion of NO_x. It is therefore desirable to have a high amount of stored NH_3. However, it is inevitable that some NH_3 leaves the catalyst without reacting with any NO_x. This is called NH_3 slip and a greater amount of stored NH_3 leads to more NH_3 slip, which is undesirable, both from a practical and economical point of view. However, it is also legislated and must be kept within certain levels. The temperature of the catalyst also affects the NH_3 slip in such a way that higher temperatures increase the NH_3 slip.

The main objective for a dosing controller is therefore to keep the amount of stored NH_3 high, without producing excessive NH_3 slip. The controller must consider both the current slip and that of the future. The latter presents a challenge, especially if the temperature of the catalyst is increased since this will lead to higher slip unless the amount of stored NH_3 is decreased, which can only be achieved through reaction with NO_x.

2.2. Energy Balance

The energy balance for the gas phase is

$$\phi \rho_g c_{p,g} \frac{\partial T_g}{\partial t} = -v_g \phi \rho_g c_{p,g} \frac{\partial T_g}{\partial x} + h_{g \leftrightarrow s} a_{g \leftrightarrow s}(T_s - T_g) \tag{6}$$

and for the substrate

$$(1-\phi)\rho_s c_{p,s} \frac{\partial T_s}{\partial t} = (1-\phi)\lambda_s \frac{\partial^2 T_s}{\partial x^2} - h_{g \leftrightarrow s} a_{g \leftrightarrow s}(T_s - T_g) + h_{s \leftrightarrow a} a_{s \leftrightarrow a}(T_a - T_s) + Q_{react} \tag{7}$$

where

$$Q_{react} = \sum_{j \in reactions} r_j \Delta H_j \tag{8}$$

is the enthalpy change caused by the reactions.

2.3. Mass Balance

The mass balance describes the conservation of species in the catalyst and is presented below.

2.3.1. Reactions

In this work, the reactions in Section 2.1.1 are considered. Ammonia adsorption and desorption rates are

$$r_{ad} = k_{ad}^0 \exp\left(-E_{ad}\left(\frac{1}{T_s} - \frac{1}{T_{ref}}\right)\right)(1 - \Theta)C_{NH_3} \tag{9}$$

and

$$r_{de} = k_{de}^0 \exp\left(-E_{de}\left(\frac{1}{T_s} - \frac{1}{T_{ref}}\right)(1 - \alpha_{de}\Theta)\right)\Theta, \tag{10}$$

respectively. HNCO hydrolysis is modeled as

$$r_{hyd} = k_{hyd}^0 \exp\left(-E_{hyd}\left(\frac{1}{T_s} - \frac{1}{T_{ref}}\right)\right)C_{HNCO}, \tag{11}$$

and the three NO_x reducing reactions are modeled as

$$r_{sdt} = k_{std}^0 \exp\left(-E_{std}\left(\frac{1}{T_s} - \frac{1}{T_{ref}}\right)\right)\theta^*\left(1 - \exp -\frac{\theta}{\theta^*}\right)C_{NO} \tag{12}$$

$$r_{fst} = k_{fst}^0 \exp\left(-E_{fst}\left(\frac{1}{T_s} - \frac{1}{T_{ref}}\right)\right)\theta C_{NO}C_{NO_2} \tag{13}$$

$$r_{slw} = k_{slw}^0 \exp\left(-E_{slw}\left(\frac{1}{T_s} - \frac{1}{T_{ref}}\right)\right)\theta C_{NO_2}. \tag{14}$$

2.3.2. Mass Balance

Based on the reactions above, the mass balances for each species become: for ammonia

$$\frac{\partial C_{NH_3}}{\partial t} = -v_g \frac{\partial C_{NH_3}}{\partial x} - r_{ad} + r_{de} + r_{hyd}, \tag{15}$$

for HNCO

$$\frac{\partial C_{HNCO}}{\partial t} = -v_g \frac{\partial C_{HNCO}}{\partial x} - r_{hyd}, \tag{16}$$

for NO

$$\frac{\partial C_{NO}}{\partial t} = -v_g \frac{\partial C_{NO}}{\partial x} - 4r_{std} - r_{fst}, \tag{17}$$

and for NO_2

$$\frac{\partial C_{NO_2}}{\partial t} = -v_g \frac{\partial C_{NO_2}}{\partial x} - r_{fst} - 6r_{slw} \tag{18}$$

The dynamics of the ammonia storage, θ, is

$$\frac{d\theta}{dt} = \frac{r_{ad} - r_{de} - 4r_{std} - 2r_{fst} - 8r_{slw}}{\Omega} \tag{19}$$

2.4. Pressure Drop

The flow in the catalyst channels is assumed to be laminar and therefore the Hagen–Poiseuille pressure drop relation

$$\frac{\partial p}{\partial x} = -\frac{F_h \mu v_g}{d_h^2} \tag{20}$$

is used to describe the relation between pressure drop and gas velocity. The dynamic viscosity of the gas is modeled as an afine function in temperature,

$$\mu = \mu_0 + \mu_1 T_g. \tag{21}$$

3. Spatial Discretization

This section describes how the PDEs are approximated as ODEs. Two different models are presented. The two models differ in the way they model gas temperature and concentrations in the catalyst, but are otherwise the same. Therefore, the common features between the models are first presented, and subsequently the specific details of each model are given.

3.1. Common Features between the Models

Here, features that are shared between the two models are presented.

3.1.1. Spatial Discretization Grid

To transform the PDE to an ODE the catalyst is first discretized lengthwise into N segments of length $\frac{L}{N}$. Each segment n has an ammonia surface coverage Θ_n and a substrate temperature $T_{s,n}$, which are both assumed constant over the segment. The output temperature

and concentration from segment n are denoted $T_{g,n}$ and C_n, respectively, and are calculated in different ways in the two models. The inputs are the output from the previous segment, i.e., $T_{g,n-1}$ and C_n, except for the first ($n = 1$) where $T_{g,1} = T_{in}$ and $C_{n-1} = C_{in}$. See Figure 1 for an illustration.
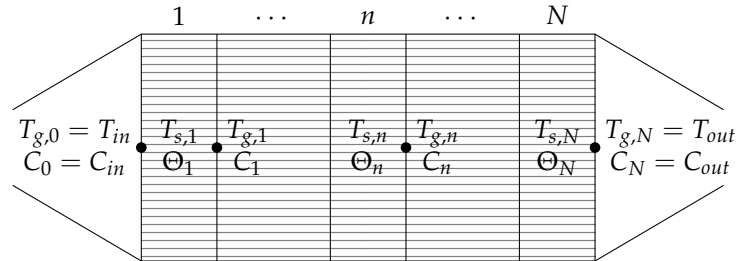

Figure 1. Illustration of the catalyst discretization.

3.1.2. Energy Balance in Substrate

Using the spatial discretization, the partial derivatives can be approximated as

$$\frac{\partial T_s}{\partial x}(t, x_n) \approx T_{s,n}^{(x)} := \begin{cases} \frac{T_{s,n-1} - T_{s,n}}{\frac{L}{N}}, & n = 2, \ldots, N \\ \frac{L}{N} h_{ff} a_{ff} (T_{pre} - T_{s,1}), & n = 1 \\ \frac{L}{N} h_{bf} a_{bf} (T_{post} - T_{s,N}), & n = N + 1 \end{cases} \quad (22)$$

and

$$\frac{\partial^2 T_s}{\partial x^2}(t, x_n) \approx T_{s,n}^{(xx)} := \frac{T_{s,n}^{(x)} - T_{s+1}^{(x)}}{\frac{L}{N}} \quad (23)$$

The two models describe the temperature of the gas in different ways, and it is therefore more convenient to calculate the heat flow between the gas and substrate using the difference between inlet and outlet temperature in the following way

$$\dot{Q}_{g\leftrightarrow s,n} = W c_{p,g}(T_{g,n-1} - T_{g,n}). \quad (24)$$

Using the above, the energy balance for the substrate can be written

$$(1 - \phi)\rho_s c_{p,s} \frac{\partial T_{s,n}}{\partial t} = (1 - \phi)\lambda_s T_{s,n}^{(xx)} + \dot{Q}_{g\leftrightarrow s,n} + h_{s\leftrightarrow a} A_{s\leftrightarrow a}(T_a - T_{s,n}) + \dot{Q}_{react,n} \quad (25)$$

3.1.3. Pressure Drop

In these implementations, exhaust mass flow, W, and pressure after the catalyst, p_{out} are employed as inputs and used to calculate the pressure inside the catalyst.

If constant gas temperature in an element is assumed, the gas velocity becomes

$$v_g = \frac{W}{\rho_g A_c} = \frac{W R_g T_g}{p A_c} \quad (26)$$

and the solution to

$$\frac{\partial p}{\partial x} = -\frac{F_h \mu v_g}{d_h^2} = -\frac{F_h \mu W R_g T_g}{p A_c d_h^2} \quad (27)$$

becomes

$$p(x) = \sqrt{2 \frac{F_h \mu W R_g T_g}{A_c d_h^2}(x - L) + p_{out}^2} \quad (28)$$

Using this, the pressure at the end of each segment can be calculated as

$$p_n = \sqrt{p_{n+1}^2 - 2\frac{F_h \mu W R_g T_{g,n}}{A_c d_h^2}\frac{L}{N}} \tag{29}$$

with $p_{N+1} = p_{out}$.

3.1.4. Compact Notation

Before continuing with deriving the models, it is useful to define

$$C = \begin{bmatrix} C_{NH_3} \\ C_{HNCO} \\ C_{NO} \\ C_{NO_2} \end{bmatrix} \tag{30}$$

so that the mass balance can be written

$$\frac{\partial C}{\partial t} = -v_g \frac{\partial C}{\partial x} + r_{tot} \tag{31}$$

where

$$r_{tot} = \begin{bmatrix} -r_{ad} + r_{de} + r_{hyd} \\ -r_{hyd} \\ -4r_{std} - r_{fst} \\ -r_{fst} - 6r_{slw} \end{bmatrix} \tag{32}$$

3.2. Continuous Stirred-Tank Reactor (CSTR)

In this model, based on the assumptions in Sections 1.1.1 and 1.1.2, the temperatures and concentrations are modeled as homogeneous in the catalyst and continuously mixed with the inlet flow.

3.2.1. Single Segment

If the catalyst is discretized using a single segment, this model becomes very simple. In this case, the gas temperature is modeled as

$$\phi \rho_g c_{p,g} \frac{dT_g}{dt} = -v_g \phi \rho_g c_{p,g} \frac{T_{in} - T_g}{L} + h_{g \leftrightarrow s} a_{g \leftrightarrow s}(T_s - T_g) \tag{33}$$

and, in the same way, the concentrations are modeled as

$$\frac{dC}{dt} = -v_g \frac{C_{in} - C}{\frac{L}{N}} + r_{tot}. \tag{34}$$

The output from the model is the homogeneous temperature and concentration T_g and C, respectively.

3.2.2. Multiple Segments

The accuracy of the model can be improved by connecting N models in series allowing the output of the previous one to be input to the next one resulting in

$$\phi \rho_g c_{p,g} \frac{dT_{g,n}}{dt} = -v_g \phi \rho_g c_{p,g} \frac{T_{g,n-1} - T_{g,n}}{\frac{L}{N}} + h_{g \leftrightarrow s} a_{g \leftrightarrow s}(T_{s,n} - T_{g,n}) \tag{35}$$

and

$$\frac{dC_n}{dt} = -v_g \frac{C_{n-1} - C_n}{\frac{L}{N}} + r_{tot}(C_n) \tag{36}$$

for each segment $n = 1, \ldots, N$.

As a side note, it is worth mentioning that this model can be seen as an implementation where the spatial derivatives have been approximated with finite differences.

3.3. Instantaneous Equilibrium in Gas Phase (IEGP)

A major disadvantage of the CSTR model is the fast dynamics that the gas transport gives rise to. Under normal operation, the mass flows through the catalyst are high and the gas phase will quickly reach an equilibrium. This is a motive to assume a quasi-static behavior, and remove the mixing dynamics from the equations, along with the other assumptions in Section 1.1.1. This results in a few changes compared to the CSTR model and they are presented below.

3.3.1. Energy Balance

Removing the mixing dynamics from the gas phase results in

$$0 = -v_g \phi \rho_g c_{p,g} \frac{\partial T_g}{\partial x} + h_{g \leftrightarrow s} a_{g \leftrightarrow s} (T_s - T_g) \tag{37}$$

which, for a constant T_s, has the solution

$$T_g(x) = (T_{in} - T_s) e^{\frac{v_g \phi \rho_g c_{p,g} x}{h_{g \leftrightarrow s} a_{g \leftrightarrow s}}} + T_s \tag{38}$$

Using the result above, the output temperature from segment n can be calculated as

$$T_{g,n} = (T_{g,n-1} - T_{s,n}) e^{\frac{v_{g,n} \phi \rho_{g,n} c_{p,g} L}{h_{g \leftrightarrow s} a_{g \leftrightarrow s} N}} + T_{s,n} \tag{39}$$

with $T_{g,0} = T_{in}$.

3.3.2. Mass Balance

Removing the mixing dynamics from the mass balance results in

$$0 = -v_g \frac{\partial C}{\partial x} + r_{tot}(C) \tag{40}$$

Due to the structure of $r_{tot}(C)$, especially the nonlinear term from the fast SCR reaction, no closed-form expression solution exists according to the authors' knowledge, and instead numerical methods must be used. By rewriting the equations on the standard form

$$\frac{\partial C}{\partial x} = \frac{1}{v_g} r_{tot}(C) \tag{41}$$

It becomes clear that since the Jacobinan matrix

$$\frac{\partial}{\partial C} \left(\frac{1}{v_g} r_{tot}(C) \right) \tag{42}$$

can have arbitrarily large eigenvalues, the problem is stiff and the solver should be chosen accordingly [29].

The Backward Euler method is one of the most simple stiff methods and its application to the problem yields the following formula for the output from segment n

$$C_n = C_{n-1} - \frac{L}{N} \frac{1}{v_n} r_{tot}(C_n) \tag{43}$$

Again, no closed-form solution exists to the above equation according to the authors' knowledge, and instead Newton's method is used to iteratively find an approximate solution. Starting with

$$C_n^0 = C_{n-1} \tag{44}$$

A better approximation is iteratively found by the formula

$$C_n^{k+1} = C_n^k - \left(\frac{\partial}{\partial C} \left(\frac{L}{Nv_g} r_{tot}(C_n^k) \right) \right)^{-1} \left(C_{n-1} + \frac{L}{Nv_n} r_{tot}(C_n^k) \right) \tag{45}$$

It was found that under normal operation, convergence only required a few iterations (typically 2–3), and therefore, choosing a fixed number of iterations instead of testing for convergence at each iteration is more efficient.

The concentrations at the outlet of the segment are calculated using only one step, however, using M steps is easily achieved by just repeating the procedure M times using the shorter step length $\frac{L}{NM}$.

3.3.3. Transport Delay

When changing the conditions at the inlet of the catalyst, it will take some time before any changes are seen at the outlet because of the time required for the gas to flow through the catalyst. When removing the mixing dynamics this effect is also removed and instead a change in inlet condition will result in an instantaneous change in the outlet conditions. In this section, an expression for the transport delay and a way to integrate it in the model are presented.

A pure transport equation has the form

$$\frac{\partial y}{\partial t}(t, x) = -v(t) \frac{\partial y}{\partial x}(t, x) \tag{46}$$

where $y(t, 0)$ is the conditions at the inlet and $y(t, L)$ is the sought after conditions at the outlet. If $v(t) = v$ is constant, the solution is

$$y(t, L) = y(t - \frac{L}{v}, 0) \tag{47}$$

However, if $v(t)$ is not constant, the problem becomes a bit more involved. To derive an expression for this case we start by dividing the length into N pieces and denote the output from each segment $y_n(t)$. If N is chosen large enough so that the time delay over each segment $\frac{L}{Nv(t)}$ small, then

$$y_n(t) \approx y_{n-1}\left(t - \frac{L}{Nv(t)} \right) \tag{48}$$

Now, by letting

$$\tau_n = \begin{cases} \sum_{k=0}^{n-1} \frac{L}{Nv(t - \tau_k)}, & n = 1, \ldots, N \\ 0 & n = 0 \end{cases} \tag{49}$$

and inserting it in (48) and continuing to unfold the recursion yields

$$\begin{aligned} y_n(t) &\approx y_{n-1}\left(t - \frac{L}{Nv(t)} \right) = y_{n-1}(t - \tau_1) \\ &\approx y_{n-2}\left(t - \tau_1 - \frac{L}{Nv(t - \tau_1)} \right) = y_{n-2}(t - \tau_2) \\ &\vdots \\ &\approx y_0(t - \tau_N) \end{aligned} \tag{50}$$

The fact that if

$$\tau(t, x) = \int_0^x \frac{L}{Nv(t - \tau(l))} dl \tag{51}$$

exists for all $x \in [0, L]$, then it holds that $\tau_N \longrightarrow \tau(x)$ as $N \longrightarrow \infty$, together with that the accuracy of the approximation should increase with a larger N motivates that

$$y(t, x) = y(t - \tau(t, x), 0) \tag{52}$$

To incorporate this in the model, the model is first simulated without considering the transport delay and the result is then post-processed using the calculated time delay.

4. Analysis of Steady-State Solutions

In this section, some properties of the models during steady state, i.e., when all time derivatives are zero, are investigated.

4.1. Comparison of Models during Steady State

During steady state, all time derivatives are zero and for the CSTR the concentration calculations becomes

$$\frac{dC_n}{dt} = 0 = -v_g \frac{C_{n-1} - C_n}{\frac{L}{N}} + r_{tot}(C_n) \Rightarrow C_n = C_{n-1} - \frac{L}{N} \frac{1}{v_n} r_{tot}(C_n) \tag{53}$$

which is identical to (43). This means that during steady state, the CSTR gives the same output as the IEGP model with one backward Euler step on each segment.

4.2. Standard SCR Example

To investigate the steady-state solutions further, a standard SCR reaction is studied. Stationary, the NO concentration is governed by

$$0 = -\frac{\partial C_{\mathrm{NO}}}{\partial x} - k_{\mathrm{NO}}^{tot} C_{\mathrm{NO}} \tag{54}$$

where

$$k_{\mathrm{NO}}^{tot} = \frac{1}{v_g} 4k_{std}^0 \exp\left(-E_{std}\left(\frac{1}{T_s} - \frac{1}{T_{ref}}\right)\right) \theta^* \left(1 - \exp{-\frac{\theta}{\theta^*}}\right) \tag{55}$$

To simplify the analysis we will assume that k_{NO}^{tot} constant and that the length of the catalyst is $L = 1$.

4.2.1. True Solution

The solution to (54) is

$$C_{\mathrm{NO},out}^{true} = C_{\mathrm{NO},in} e^{-k_{\mathrm{NO}}^{tot}} \tag{56}$$

for a catalyst of length $L = 1$.

4.2.2. Solution Using Backward Euler

Applying the backward Euler scheme from (53) to (54) yields

$$C_{\mathrm{NO},n} = C_{\mathrm{NO},n-1} - \frac{k_{\mathrm{NO}}^{tot}}{N} C_{\mathrm{NO},out} \Rightarrow C_{\mathrm{NO},n} = C_{\mathrm{NO},n-1} \frac{1}{1 + \frac{k_{\mathrm{NO}}^{tot}}{N}} \tag{57}$$

and thus

$$C_{\mathrm{NO},out}^{eb} = C_{\mathrm{NO},in} \frac{1}{\left(1 + \frac{k_{\mathrm{NO}}^{tot}}{N}\right)^N}. \tag{58}$$

4.2.3. Tuning Parameter

Applying backward Euler to a problem of this type will lead to an underestimation of the decay, and it is therefore reasonable to assume that a tuning constant $\gamma \geq 1$ entering linearly with k_{NO}^{tot} could improve the result. With this tuning constant, the solution using the backward Euler scheme becomes

$$C_{\text{NO},out}^{eb} = C_{\text{NO},in} \frac{1}{\left(1 + \gamma \frac{k_{\text{NO}}^{tot}}{N}\right)^N}. \tag{59}$$

4.2.4. Relation between Reaction Rate and Conversion Efficiency

The efficiency of the conversion can be defined as

$$\eta = 1 - \frac{C_{\text{NO},out}}{C_{\text{NO},in}} = 1 - e^{-k_{\text{NO}}^{tot}} \tag{60}$$

and thus

$$k_{\text{NO}}^{tot} = -\ln(1 - \eta). \tag{61}$$

4.2.5. Relative Error

The relative error, when comparing with the true solution, is

$$\epsilon = \frac{C_{\text{NO},in} e^{-k_{\text{NO}}^{tot}} - C_{\text{NO},in} \frac{1}{\left(1 + \gamma \frac{k_{\text{NO}}^{tot}}{N}\right)^N}}{C_{\text{NO},in} e^{-k_{\text{NO}}^{tot}}} = 1 - \frac{e^{k_{\text{NO}}^{tot}}}{\left(1 + \gamma \frac{k_{\text{NO}}^{tot}}{N}\right)^N} \tag{62}$$

and only depends on k_{NO}^{tot} and N. Using the relationship between k_{NO}^{tot} and η in (61), the relative error can be rewritten in terms of η as

$$\epsilon = 1 - \frac{e^{-\ln(1-\eta)}}{\left(1 - \gamma \frac{\ln(1-\eta)}{N}\right)^N} = 1 - \frac{(1-\eta)^{-1}}{\left(1 - \gamma \frac{\ln(1-\eta)}{N}\right)^N} \tag{63}$$

to ease the interpretation.

5. Temporal Discretization

To handle input data and simulate the ODE:s using a computer, temporal discretization is necessary. This section describes how this is achieved.

5.1. Input Data

Most of the data used as input to the model are equidistantly sampled with sampling time 0.1 s. Therefore, in this paper a sampling time of $\Delta t_s = 0.1$ s is used and the problem becomes to successively solve the ODE:s over this time period.

5.2. CSTR

The mixing dynamics in the CSTR model are very fast, especially for high gas velocities, and therefore, a solver with variable step size for stiff systems is appropriate. In general, a tailored method for the specific problem is the best choice. However, it is also demanding to produce such methods that can compete with commercial software. Because of this, Simulink and its numerical differentiation formulas are used to solve the ODE:s from the CSTR model.

5.3. IEGP

After removing the mixing dynamics, the remaining dynamics are very slow when compared to the sampling time of 0.1 s. This makes it possible to use the forward Euler method to solve the ODE:s, i.e.,

$$\begin{bmatrix} T_{s,n}(t + T_s) \\ \Theta_n(t + T_s) \end{bmatrix} = \begin{bmatrix} T_{s,n}(t) + \Delta t_s \frac{\partial T_{s,n}}{\partial t}(t) \\ \Theta_n(t) + \Delta t_s \frac{\partial \theta_n}{\partial t}(t) \end{bmatrix}. \tag{64}$$

6. Model Generation Tool

To ease the implementation of different catalyst models, a tool that automatically generates them is developed in Matlab. The tool works by letting the user define the inputs described in Table 1 which the tool employs to create symbolic expressions of all equations in Section 3. The symbolic expressions are then used to create a file which implements them, together with a struct of all parameters needed to run it. An example can be seen in Appendix A, where the code generating the SCR model is presented.

Given the general structure of the equations and the tool, it is possible to use the tool to model most types of catalysts. In particular, with the tool it is also possible to generate models of diesel oxidation catalysts and ammonia slip catalyst, meaning that a complete NO_x reduction system can be modeled.

Table 1. Inputs for the model generation tool.

Name	Description
Species	Vector of species
→ Name	String with name of species
→ Subscript	String with subscript of species
Sites	Vector of sites
→ Name	String with name of site
→ Subscript	String with subscript of site
Reactions	Vector of reactions
→ Name	String with name of reaction
→ Subscript	String with subscript of reaction
→ Reactants	Struct with info. of reactant molar ratios
→gaseous	Vector of molar ratios for each species
→adsorbed	Vector of molar ratios for each site
→ Products	Struct with info. of product molar ratios
→gaseous	Vector of molar ratios for each species
→adsorbed	Vector of molar ratios for each site
→ Kinetics	Function handle calculating reaction rate
→ Parameters	Parameters for the reaction rate calculation
Options	Struct with options
→ Discretization	String specifying type of discretization
→ Conc. calc.	Struct specifying how output conc. is calc.
→ Model name	String specifying name of generated model

7. Parameterization and Validation

The equations in Section 2 are used extensively in the literature and have been verified in numerous publications [2,16,25–28]. Therefore, the main objective here is to verify the accuracy of the implementations in Section 3 and estimate and validate the parameters in them. This is achieved by both using data from a high-fidelity model and also by comparing the two models. When comparing the models it is assumed that when a large number of segments are used in the discretionary, the CSTR model should give a solution that is close to the true solution.

7.1. Data

The data used to estimate parameters and validate the model come from simulations of a high-fidelity model and are presented in Table 2.

Table 2. Data used for parameterization and validation.

Data	Description
A	FTP cycle without any reactive species (only C_{02} and air).
B	A cycle with steps in ammonia dosing at different temperatures without any other reactive species.
C	FTP cycle with all species.
D	WHTC cycle with all species. Inputs are shown in Figure 2
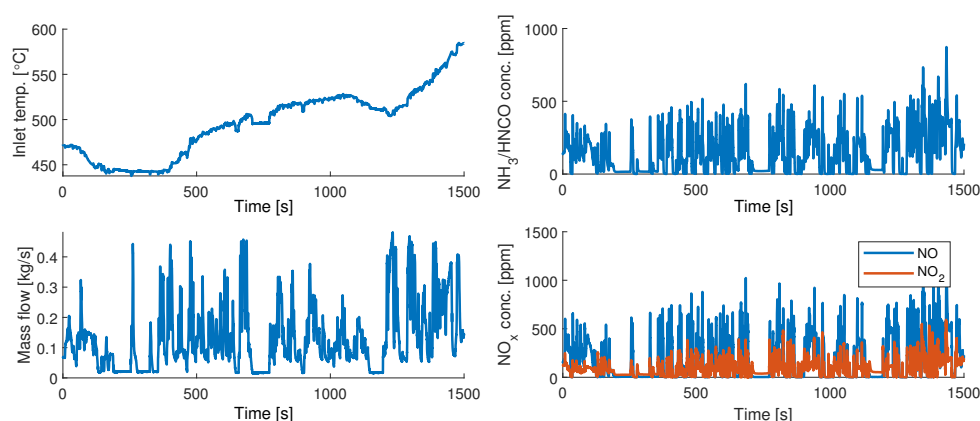
Figure 2. Inputs from the WHTC drive cycle.

7.2. Parameter Estimation

Most parameters in the models are taken from data sheets of the specific system and tables of physical constants and materials. To estimate the remaining parameters, *fminsearch* in MATLAB is used. To create a cost to minimize, the model is simulated using the same inputs as the high-fidelity model and the error compared to the high-fidelity model is calculated. Due to long simulation times of the CSTR model, only the IEGP model is used to estimate parameters and these parameters are used in both models. Since there are dependencies between the parameters they are estimated in the following five steps:

Step 1 Data A is used estimate all the convective heat transfer coefficients h, thermal conductivity of the substrate λ_s, and specific heat capacities c_p. Mean square error of the output temperature is used as cost function.

Step 2 Data A is used to estimate the friction factor in the pressure drop model F_h, and the slope of the dynamic viscosity model μ_1. Mean square error of the input pressure is used as cost function.

Step 3 Data B is used to parameterize the ammonia storage model. Estimated parameters are: k_{ad}^0, k_{de}^0, E_{ad}, E_{de}, α_{de}, Ω. Mean square error of output concentrations are used as cost function.

Step 4 Data C is used to parameterize the rest of the parameters in the chemical model. Mean square error of output concentrations are used as cost function.

Step 5 Data C is used to tune all previously estimated parameters. The sum of all previous cost functions, normalized with their lowest individual values, are used as cost function.

The steps above were also carried out for models with different number of segments N in the discretization to investigate how this affects performance.

To validate the model, it was compared to the high-fidelity model using data set D.

8. Results

In this section, the results from the validation and comparison of the models are shown. In all simulations used to produce data in this section, the inputs from the WHTC cycle given in Figure 2 are used.

8.1. Parameter Estimation

First, different values of the number of segments in the discretization, N, the number of backward Euler steps on each segment, M, and the number of Newton iterations in each backward Euler step, K, were manually chosen and used to estimate parameters in the model, following the procedure in Section 7.2. It was found that $N = 30$, $M = 2$, and $K = 4$ gave good results, and increasing either parameter did not improve the results significantly. Due to confidentiality, the result of the parameter estimation cannot be presented. However, it can be reported that the output from the model was very close to that of the high-fidelity model. Notably, it was closer than these types of models generally fit measurements from real systems, such as [15,16].

Validation

To further investigate the accuracy of the parameters estimated using $N = 30$, $M = 2$, and $K = 4$, Figures 3–5 were created by simulating the model using these parameters for different N, M, and K, and comparing the results.

First, the number of Newton iterations needed for convergence is investigated in Figure 3. Here it can be seen that convergence seems to be achieved for a K between four and six for the investigated values of N. It can also be seen that for $K \geq 4$ the error is only a fraction of a PPM which is considered to be very low.
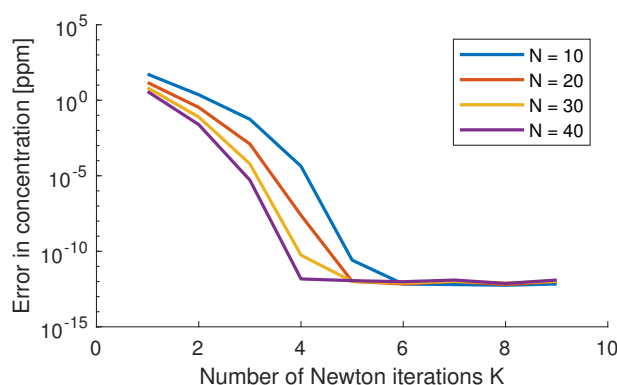

Figure 3. Maximal instantaneous error of any output concentration for different number of Newton iterations K and number of segments N. Simulation with $K = 10$ for respective N is used as reference.

In Figure 4, it can be seen that the maximal instantaneous error in output temperature decreases rapidly when N is increased from one. However, there is a knee around $N = 10$ after which the improvement becomes slower. It can also be seen that going beyond $N = 30$ does not yield any significant improvements.

Figure 5 shows the maximal instantaneous error in output concentrations for different N and M. Here a the same trend when increasing N as for output temperature can be seen. For the parameter M it can bee seen that increasing it from one to two yields quite some improvements, but increasing it further does not seem to improve the results significantly, except for NO_2.

From this it can be concluded that simulations using $N = 30$, $M = 2$, and $K = 4$ provide a result very close to the best possible, and therefore the parameters estimated using them are employed in the rest of the paper.
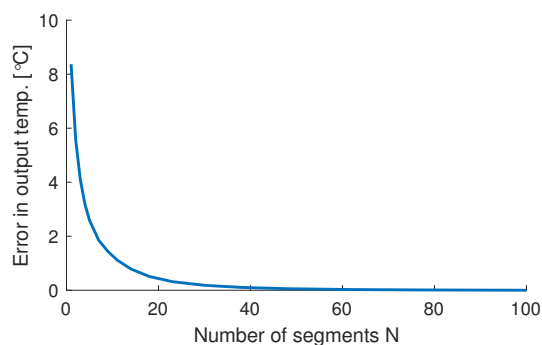
Figure 4. Maximal instantaneous error in output temperature for different numbers of N. Results from simulation with $N = 100$ is used as reference.
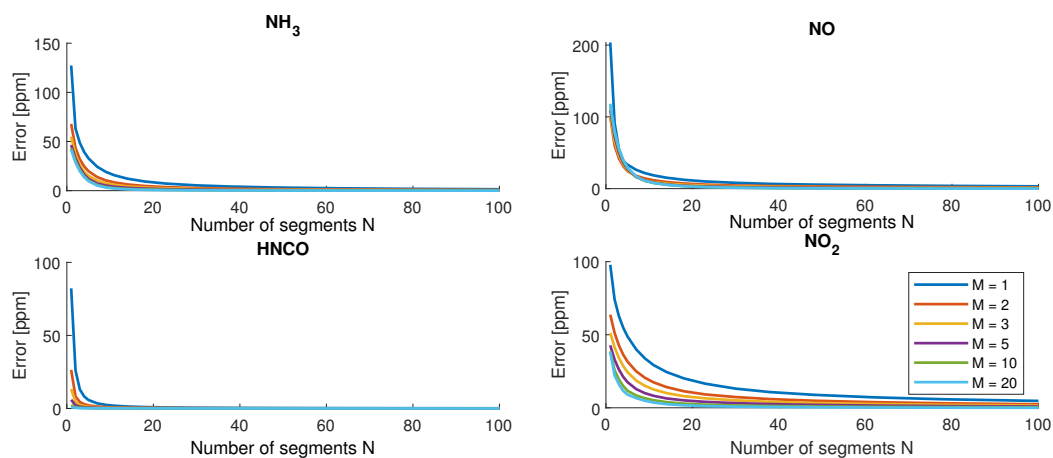

Figure 5. Maximal instantaneous error in output concentrations for different numbers of N and M. Results from simulation with $N = 100$ and $M = 20$ are used as reference.

8.2. Model Comparison

In this section, the two models are compared, both in terms of accuracy and simulation time.

Model Accuracy

Figure 6 shows the maximal instantaneous error for all outputs among all models and different N. Here, it can be seen that for output temperature the result is quite similar for the CSTR model and the IEGP model for $N \leq 30$. For larger N, it appears the CSTR gives slightly better results. However, this might come from the fact that CSTR with $N = 100$ is used as reference and that its output is not close enough to the true solution to draw any conclusions for larger N. The IEGP model with time delay is also represented in the figure, however, it does not improve the results, in fact it produces worse results for $N \geq 10$. The reason for this is that at low mass flows, the output temperature will be closer to the substrate temperature than at higher mass flows due to the longer time the gas stays in the substrate. This means that rapid changes in mass flow, without changing the input temperature, can result in changes in the output temperature and the changes are not affected by the transport delay in the same way as when the input temperature is changed. This can be seen in Figure 7, where it can be observed that the rapid change in mass flow creates almost as rapid a change in output temperature using the CSTR model, and the time delay used in the IEGP model does not produce similar results. Figure 7 also shows why the time-delayed model becomes worse at $N = 10$, as can be seen the temperature from the model with $N = 5$ is too high before the change and too low after. This means that during the step the error does not become as large as for the model with $N = 10$.
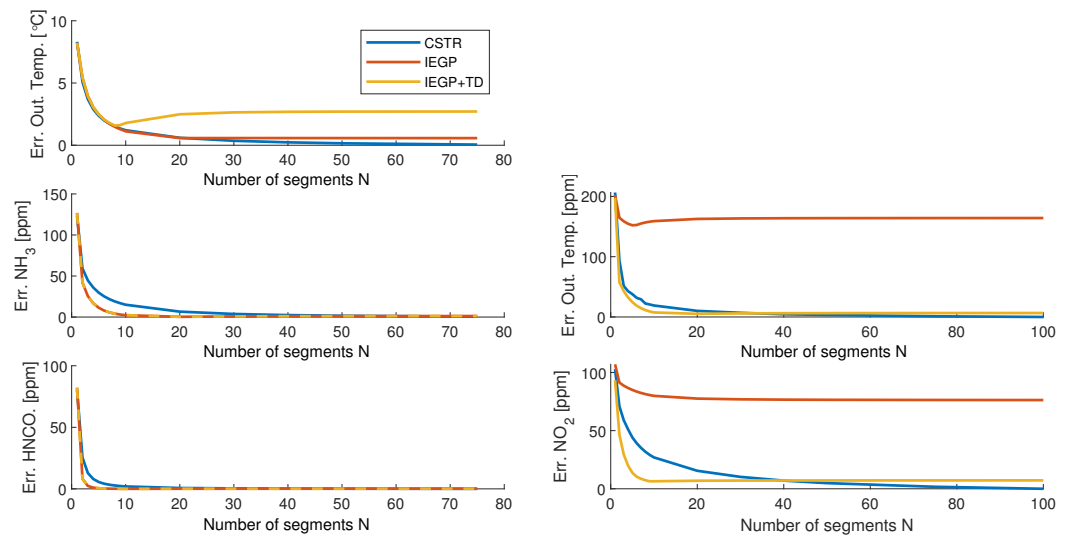
Figure 6. Maximal instantaneous error for all outputs among all models and different N. For the IEGP models, $M = 2$ and $K = 5$ were used. The CSTR with $N = 100$ was used as reference.
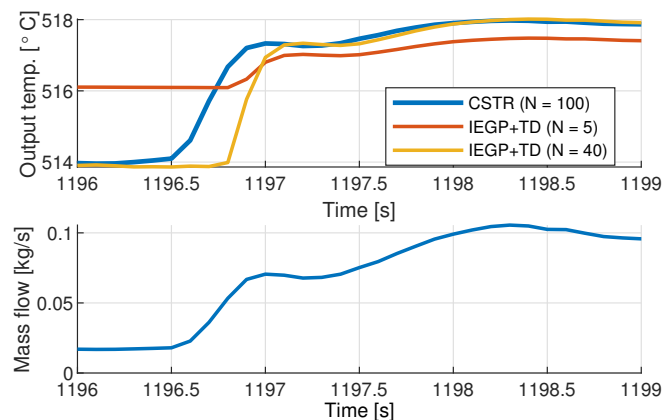

Figure 7. Output temperature for different models during a rapid change in mass flow.

When looking at the output concentrations in Figure 6, larger differences can be seen. For $N = 1$ the results are very similar, but for $1 < N \le 40$ the time-delayed IEGP model shows significantly better results. However, without the time delay the IEGP model does not show good results. This is because small time delays can bear a huge effect on the instantaneous error in transients. This can be seen in Figure 8 where the IEGP model with and without time delay is compared to the CSTR model. As can be seen, with the time delay the IEGP model produces almost identical output as the CSTR model, but without the time delay it is a fraction of a second before thus resulting in large instantaneous differences.
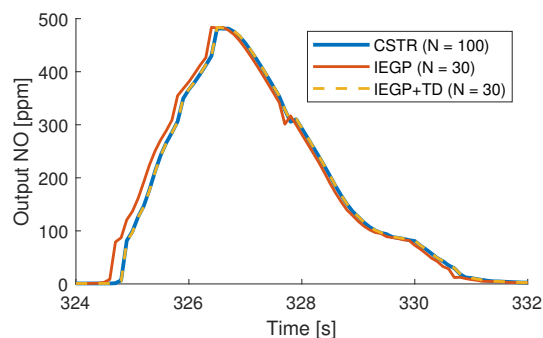

Figure 8. Output NO for a part of the WHTC cycle for three different models.

To circumvent the problems with instantaneous errors in validation, Figure 9 is used. Here, the average error in output NO_2 for different window sizes is presented. Moreover, it can be seen here that the average error quickly becomes smaller when the window size is increased, and when looking at the 20 s average the IEGP model with and without time delay produces quite similar results.
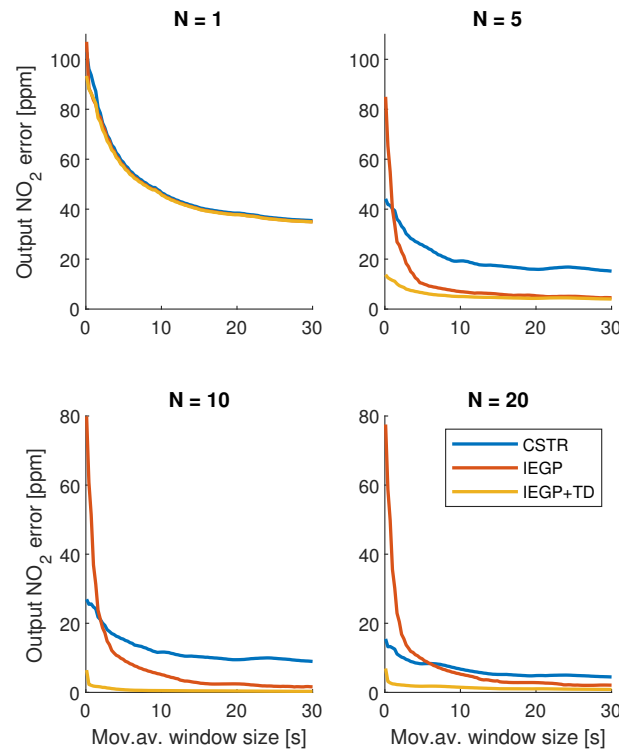

Figure 9. Maximal average error in output NO_2 for different window sizes in the three different models and different N.

8.3. Simulation Time

Figure 10 shows simulation times for the two models for different N. As can be seen, the IEGP is around 100-times faster than the CSTR model and its simulation times are also increased less when N is increased.
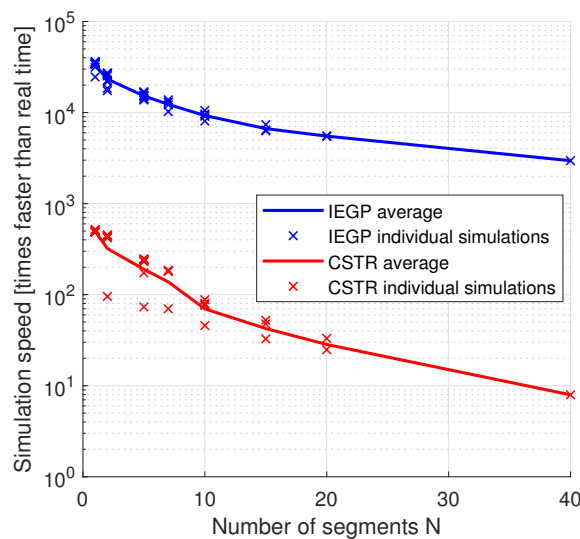

Figure 10. Simulation speed of the two models for different N. In the IEGP model. $M = 2$ and $K = 5$ were used.

9. Conclusions

Two models of an SCR catalyst, CSTR and IEGP, have been presented, validated and compared with each other. Both models are based on the same set of equations describing the physics of the catalyst, and only differ in the way they handle the transport of gases within the catalyst. It is also shown that around 20 segments in the discretization provides a good trade-off between simulation time and accuracy.

The IEGP model outperforms the CSTR when using a reasonable number of segments in the discretization (less than 40), both in accuracy and simulation time. The difference in accuracy is largest for around five segments in the discretization, where the IEGP model is around five-times more accurate regarding outlet NO_x error. The simulation times are around 100-times faster for the IEGP model.

The IEGP model handles the transport of gases within the catalyst by removing the delay in output normally caused by the transport. A method to calculate this delay and post-process the output to incorporate the delay is presented. It is shown that this gives good results for the output concentrations; however, the output temperature should not be delayed.

A tool for generating the models has also been presented. The tool is general in nature and can be used to generate models of many catalyst types, and in particular a complete NO_x reduction system can be modeled.

10. Discussion

One conclusion of this work is that the IEGP model outperforms the CSTR model. It should be noted that this refers to the type of simulation used in this work and the specific implementations of the models. It is possible that the CSTR model can excel in other applications or be implemented in a more efficient way.

Furthermore, it should be noted that all the simulations are performed using the same set of parameters, and it is possible that different parameters could yield better results when the number of segments in the model is decreased. However, if different parameters are used, the validity of the equations in Section 2 can no longer be used to support the validity of the model to the same extent.

Nomenclature and Subscripts

The following nomenclature and subscripts are used in this work

Symbol	Description
α_{de}	Desorption activation energy factor
λ	Thermal conductivity
μ	Dynamic viscosity
ρ	Density
ϕ	Porosity
a	Area per length unit
A	Area
c_p	Specific heat capacity at constant pressure
C	Concentration
d	Diameter
E	Activation energy
F_h	Friction factor
h	Convective heat transfer coefficient
H	Enthalpy
k^0	Pre-exponential factor
K	Number of Newton iterations
L	Length
M	Number of backward Euler steps per segment
N	Number of segments in discretization
p	Pressure
Q	Heat
r	Reaction rate
R	Specific gas constant
t	Time
T	Temperature
v	Velocity
W	Mass flow

Subscript	Description
ad	Adsorption
c	Channels
de	Desorption
fst	Fast (SCR)
g	Gas
h	Hydraulic
hyd	Hydrolysis
in	In/inlet
out	Out/outlet
$react$	Reaction
ref	Reference
s	Substrate
slw	Slow (SCR)
std	Standard (SCR)
tot	Total

Appendix A. MATLAB Example Code

```matlab
1   % Species
2   %=================================================
3   species(1).name = 'Ammonia';
4   species(1).subscript = 'NH3';
5   species(2).name = 'HNCO';
6   species(2).subscript = 'HNCO';
7   species(3).name = 'NO';
8   species(3).subscript = 'NO';
9   species(4).name = 'NO_2';
10  species(4).subscript = 'NO2';
11  % Sites
12  %=================================================
13  sites(1).name = 'Ammonia';
14  sites(1).subscript = 'NH3';
15  sites(1).storage_capacity = 535.789750171981;
16  % Reactions
17  %=================================================
18  % Adsorption
19  reactions(1).name = 'Adsorption';
20  reactions(1).subscript = 'Ad';
21  reactions(1).reactants.gaseous  = [1;0;0;0];
22  reactions(1).reactants.adsorbed =  0;
23  reactions(1).products.gaseous  = [0;0;0;0];
24  reactions(1).products.adsorbed =  1;
25  reactions(1).parameters = [1;1];
26  reactions(1).kinetics = @(T,C,theta,par)  par(1)*exp(-par(2)*(1/T-1/600))*(1-theta)*C(1);
27  % Desorption
28  reactions(2).name = 'Desorption';
29  reactions(2).subscript = 'De';
30  reactions(2).reactants.gaseous  = [0;0;0;0];
31  reactions(2).reactants.adsorbed =  1;
32  reactions(2).products.gaseous  = [1;0;0;0];
33  reactions(2).products.adsorbed =  0;
34  reactions(2).parameters = [1;1];
35  reactions(2).kinetics = @(T,C,theta,par) par(1)*exp(-par(2)*(1/T-1/600)*(1-par(3)*theta))*
        theta;
36  % Standard SCR
37  reactions(3).name = 'Standard SCR';
38  reactions(3).subscript = 'Std';
39  reactions(3).reactants.gaseous  = [0;0;1;0;];
40  reactions(3).reactants.adsorbed =  1;
41  reactions(3).products.gaseous  = [0;0;0;0];
42  reactions(3).products.adsorbed =  0;
43  reactions(3).parameters = [1;1;1];
44  reactions(3).kinetics = @(T,C,theta,par) par(1)*exp(-par(2)*(1/T-1/600))*par(3)*(1-exp(-theta
        /par(3)))*C(3)
45  % Fast SCR
46  reactions(4).name = 'Fast SCR';
47  reactions(4).subscript = 'Fst';
48  reactions(4).reactants.gaseous  = [0;0;1;1];
49  reactions(4).reactants.adsorbed =  2;
50  reactions(4).products.gaseous  = [0;0;0;0];
51  reactions(4).products.adsorbed =  0;
52  reactions(4).parameters = [1;1];
53  reactions(4).kinetics = @(T,C,theta,par)  par(1)*exp(-par(2)*(1/T-1/600))*theta*C(3)*C(4);
54  % Slow SCR
55  reactions(5).name = 'Slow SCR';
56  reactions(5).subscript = 'Slw';
57  reactions(5).reactants.gaseous  = [0;0;0;6];  reactions(5).reactants.adsorbed =  8;
58  reactions(5).products.gaseous  = [0;0;0;0];  reactions(5).products.adsorbed =  0;
59  reactions(5).parameters = [1;1];
60  reactions(5).kinetics = @(T,C,theta,par) par(1)*exp(-par(2)*(1/T-1/600))*theta*C(4);
61  % HNCO Hydralisation
62  reactions(6).name = 'HNCO Hydralisation';
63  reactions(6).subscript = 'Hyd';
64  reactions(6).reactants.gaseous  = [0;1;0;0];  reactions(6).reactants.adsorbed =  0;
65  reactions(6).products.gaseous  = [1;0;0;0];  reactions(6).products.adsorbed =  0;
66  reactions(6).parameters = [1;1];
67  reactions(6).kinetics=@(T,C,theta,par) par(1)*exp(-par(2)*(1/T-1/600))*C(2);
68  % Options
69  %=================================================
70  options.discretization = 'FD'; % CSTR
71  options.cons_int.type = 'EB'; % BDF
72  options.cons_int.EB.eb_steps = 1;
73  options.cons_int.EB.newton_iterations = 4;
74  model_name = 'SCR_model_gen';
75  % Generate model
76  %=================================================
77  par = generate_catalyst_model(model_name,species,sites,reactions,options);
```

References

1. Martinovic, F.; Castoldi, L.; Deorsola, F.A. Aftertreatment technologies for diesel engines: An overview of the combined systems. *Catalysts* **2021**, *11*, 653. [CrossRef]
2. Winkler, C.; Flörchinger, P.; Patil, M.; Gieshoff, J.; Spurk, P.; Pfeifer, M. *Modeling of SCR DeNOx Catalyst-Looking at the Impact of Substrate Attributes*; Technical Report; SAE Technical Paper; SAE International: Warrendale, PA, USA, 2003.
3. Yun, B.K.; Kim, M.Y. Modeling the selective catalytic reduction of NOx by ammonia over a Vanadia-based catalyst from heavy duty diesel exhaust gases. *Appl. Therm. Eng.* **2013**, *50*, 152–158. [CrossRef]
4. Lim, S.; Lee, B.; Choi, S.; Kim, Y.; Lee, J.M. Automated Model Calibration for Urea-SCR Systems Using Test-Rig Data. *Ind. Eng. Chem. Res.* **2022**, *61*, 13523–13531. [CrossRef]
5. Metkar, P.S.; Harold, M.P.; Balakotaiah, V. Experimental and kinetic modeling study of NH3-SCR of NOx on Fe-ZSM-5, Cu-chabazite and combined Fe-and Cu-zeolite monolithic catalysts. *Chem. Eng. Sci.* **2013**, *87*, 51–66. [CrossRef]
6. Chundru, V.R. Development of a 2D SCR Catalyst on a Diesel Particulate Filter Model For Design and Control Applications to a Ultra Low NOx Aftertreatment System. Ph.D. Thesis, Michigan Technological University, Houghton, MI, USA, 2019.
7. Chundru, V.R.; Mahadevan, B.S.; Johnson, J.H.; Parker, G.G.; Shahbakhti, M. Development of a 2D Model of a SCR Catalyst on a DPF. *Emiss. Control Sci. Technol.* **2019**, *5*, 133–171. [CrossRef]
8. Hsieh, M.F.; Wang, J. Observer-based estimation of selective catalytic reduction catalyst ammonia storage. *Proc. Inst. Mech. Eng. Part D J. Automob. Eng.* **2010**, *224*, 1199–1211. [CrossRef]
9. Wei, L.; Yan, F.; Hu, J.; Xi, G.; Liu, B.; Zeng, J. Nox conversion efficiency optimization based on NSGA-II and state-feedback nonlinear model predictive control of selective catalytic reduction system in diesel engine. *Appl. Energy* **2017**, *206*, 959–971. [CrossRef]
10. Ma, Y.; Wang, J. A predictive control method for automotive selective catalytic reduction systems. In Proceedings of the 2019 American Control Conference (ACC), Philadelphia, PA, USA, 10–12 July 2019; pp. 1593–1598.
11. Chen, P.; Wang, J. Estimation and adaptive nonlinear model predictive control of selective catalytic reduction systems in automotive applications. *J. Process. Control* **2016**, *40*, 78–92. [CrossRef]
12. Sowman, J.; Laila, D.S.; Fussey, P.; Truscott, A.; Cruden, A.J. Nonlinear model predictive control applied to multivariable thermal and chemical control of selective catalytic reduction aftertreatment. *Int. J. Engine Res.* **2019**, *20*, 1017–1024. [CrossRef]
13. Hsieh, M.F.; Wang, J. Development and experimental studies of a control-oriented SCR model for a two-catalyst urea-SCR system. *Control Eng. Pract.* **2011**, *19*, 409–422. [CrossRef]
14. Gundlapally, S.R.; Papadimitriou, I.; Wahiduzzaman, S.; Gu, T. Development of ECU capable Grey-box models from detailed models—Application to a SCR reactor. *Emiss. Control Sci. Technol.* **2016**, *2*, 124–136. [CrossRef]
15. Olsson, L.; Sjövall, H.; Blint, R.J. A kinetic model for ammonia selective catalytic reduction over Cu-ZSM-5. *Appl. Catal. B Environ.* **2008**, *81*, 203–217. [CrossRef]
16. Cloudt, R.; Saenen, J.; van den Eijnden, E.; Rojer, C. *Virtual Exhaust Line for Model-Based Diesel Aftertreatment Development*; Technical Report; SAE Technical Paper; SAE International: Warrendale, PA, USA, 2010.
17. Schär, C.; Onder, C.; Geering, H. Modeling and control of an SCR system. *IFAC Proc. Vol.* **2004**, *37*, 355–360. [CrossRef]
18. Schar, C.M.; Onder, C.H.; Geering, H.P. Control of an SCR catalytic converter system for a mobile heavy-duty application. *IEEE Trans. Control Syst. Technol.* **2006**, *14*, 641–653. [CrossRef]
19. Chiang, C.J.; Kuo, C.L.; Huang, C.C.; Lee, J.Y. Model predictive control of SCR aftertreatment system. In Proceedings of the 2010 5th IEEE Conference on Industrial Electronics and Applications, Taichung, Taiwan, 15–17 June 2010; pp. 2058–2063.
20. Ritzmann, J.; Lins, G.; Onder, C. Optimization method for the energy and emissions management of a hybrid electric vehicle with an exhaust aftertreatment system. *IFAC-PapersOnLine* **2020**, *53*, 13797–13804. [CrossRef]
21. Willems, F.; Cloudt, R.; Van Den Eijnden, E.; Van Genderen, M.; Verbeek, R.; de Jager, B.; Boomsma, W.; van den Heuvel, I. *Is Closed-Loop SCR Control Required to Meet Future Emission Targets?* Technical Report; SAE Technical Paper; SAE International: Warrendale, PA, USA, 2007.
22. Donkers, M.; Van Schijndel, J.; Heemels, W.; Willems, F. Optimal control for integrated emission management in diesel engines. *Control Eng. Pract.* **2017**, *61*, 206–216. [CrossRef]
23. Suarez-Corredor, A.F.; Bäbler, M.U.; Olsson, L.; Skoglundh, M.; Westerberg, B. Understanding the NH3 adsorption mechanism on a vanadium-based SCR catalyst: A data-driven modeling approach. *Chem. Eng. Sci.* **2022**, *262*, 117975. [CrossRef]
24. Faghihi, E.M.; Shamekhi, A.H. Development of a neural network model for selective catalytic reduction (SCR) catalytic converter and ammonia dosing optimization using multi objective genetic algorithm. *Chem. Eng. J.* **2010**, *165*, 508–516. [CrossRef]
25. Chatterjee, D.; Burkhardt, T.; Rappe, T.; Güthenke, A.; Weibel, M. Numerical simulation of DOC+ DPF+ SCR systems: DOC influence on SCR performance. *SAE Int. J. Fuels Lubr.* **2008**, *1*, 440–451. [CrossRef]
26. van den Eijnden, E.; Cloudt, R.; Willems, F.; van der Heijden, P. *Automated Model Fit Tool for SCR Control and OBD Development*; SAE International: Warrendale, PA, USA, 2009. [CrossRef]
27. Koebel, M.; Elsener, M.; Kleemann, M. Urea-SCR: A promising technique to reduce NOx emissions from automotive diesel engines. *Catal. Today* **2000**, *59*, 335–345. [CrossRef]
28. Nova, I.; Lietti, L.; Tronconi, E.; Forzatti, P. Transient response method applied to the kinetic analysis of the DeNOx–SCR reaction. *Chem. Eng. Sci.* **2001**, *56*, 1229–1237. [CrossRef]
29. Shampine, L.F.; Gear, C.W. A user's view of solving stiff ordinary differential equations. *SIAM Rev.* **1979**, *21*, 1–17. [CrossRef]